CORE
Metadata, citation and similar papers at core.ac.uk
Provided by University of Strathclyde Institutional Repository

Pascal, E. and Hourahine, B. and Naresh-Kumar, G. and Mingard, K. and Trager-Cowan, C. (2018) Dislocation contrast in electron channelling contrast images as projections of strain-like components. Materials Today: Proceedings, 5 (Issue). 14652–14661. ISSN 2214-7853 , http://dx.doi.org/10.1016/j.matpr.2018.03.057

This version is available at https://strathprints.strath.ac.uk/63048/

Strathprints is designed to allow users to access the research output of the University of Strathclyde. Unless otherwise explicitly stated on the manuscript, Copyright © and Moral Rights for the papers on this site are retained by the individual authors and/or other copyright owners. Please check the manuscript for details of any other licences that may have been applied. You may not engage in further distribution of the material for any profitmaking activities or any commercial gain. You may freely distribute both the url (https://strathprints.strath.ac.uk/) and the content of this paper for research or private study, educational, or not-for-profit purposes without prior permission or charge.

Any correspondence concerning this service should be sent to the Strathprints administrator: strathprints@strath.ac.uk

The Strathprints institutional repository (https://strathprints.strath.ac.uk) is a digital archive of University of Strathclyde research outputs. It has been developed to disseminate open access research outputs, expose data about those outputs, and enable the management and persistent access to Strathclyde's intellectual output.

Available online at www.sciencedirect.com

ScienceDirect

Materials Today: Proceedings 5 (2018) 14652–14661

www.materialstoday.com/proceedings

EDS 2016

Dislocation contrast in electron channelling contrast images as projections of strain-like components

E. Pascal[a1], B. Hourahine[a], G. Naresh-Kumar[a], K. Mingard[b], C. Trager-Cowan[a]

[a] *Department of Physics, SUPA, University of Strathclyde, John Anderson Building, 107 Rottenrow, Glasgow G4 0NG, United Kingdom*
[b] *National Physics Lab, Hampton Road, Teddington, London TW11 0LW, United Kingdom.*

Abstract

The forward scattering geometry in the scanning electron microscope enables the acquisition of electron channelling contrast imaging (ECCI) micrographs. These images contain diffraction information from the beam of electrons "channelling in" to the sample. Since small, localised strains strongly affect the electron diffraction, defects which introduce lattice displacement in the region of the surface the electron beam is interacting with will be revealed as distinct variation in backscattered electron intensity. By acquiring multiple images from the same area in different diffraction conditions and comparing them against modelled predictions of defect strain sampled by diffraction, it is possible to characterise these defects. Here we discuss the relation between the elastic strain introduced by a threading dislocation intersecting the surface and the contrast features observed in the electron channelling contrast image of that region. Preliminary simulated channelling contrast images are shown for dislocations with known line direction and Burgers vectors using a two-beam dynamical diffraction model. These are demonstrated to be in qualitative agreement with measured images of dislocated polar wurtzite GaN acquired with two different diffraction conditions.

Selection and/or Peer-review under responsibility of Extended Defects In Semiconductors 2016 (EDS 2016).

Keywords: Electron channelling contrast imaging (ECCI), Dislocations, Scanning electron microscope (SEM), Image simulation, Defect imaging.

---

1. Introduction

Group III nitrides systems have proved to be particularly attractive materials for the fabrication of optoelectronic devices. Threading dislocations (TDs) are common native defects in these materials, introduced through bulk heteroepitexial growth on a lattice mismatched substrate. These extended defects propagate through the layer and

---

[1] * Corresponding author. *E-mail address:* elena.pascal@strath.ac.uk

Selection and/or Peer-review under responsibility of Extended Defects In Semiconductors 2016 (EDS 2016).

can harm the properties of the carefully engineered material. For instance, high densities of TDs have been linked to luminescence output reduction and efficiency drop in GaN-based components [1].

Nomenclature

TD	threading dislocation
a	pure edge
c	pure screw
ECCI	electron channelling contrast imaging
g	diffraction vector
s_g	deviation parameter
β	strain-like correction to s_g due to the presence of defects

The next generation of nitride semiconductor devices will require a better understanding of the origin, properties and dynamics of the various TD types. For polar wurtzite GaN, which is grown in (0001) oriented layers, the general line direction of these dislocations is also along [0001]. Two extreme dislocation characters can be distinguished: pure screw type (or **c**-type**)** where the Burgers vector (**b**) is aligned along the *c* axis and pure edge dislocation (or **a**-type) when the Burgers vector is confined to the (0001) basal plane. If neither of these conditions is strictly met, the dislocation is called mixed, or **a**+**c** type.

Transmission electron microscopy (TEM) has established itself as the default technique for the study of lattice deformations. It is especially reliable as a dislocation characterisation method as it can identify unambiguously the **c** and **a** components of a dislocation line running parallel to the imaged surface. This is achieved through the application of certain relationships between the diffraction vector **g**, Burgers vector **b** and the direction of the dislocation line $\mathbf{u_l}$ ($\mathbf{g} \cdot \mathbf{b} = 0$ and $\mathbf{g} \cdot \mathbf{b} \times \mathbf{u_l} = 0$), known as the invisibility criteria, for which no contrast associated with **c** or **a** components, respectively, can be observed. This method has been applied broadly in the study and characterisation of dislocations in cross sectional GaN samples (e.g. [2]).

For TDs which penetrate the sample surface normally (or almost normally) high resolution TEM (HRTEM) can provide direct observation of the Burgers vector direction of **a** type TDs. However, as the images are usually acquired in plan view, the **c**-components are invisible. The destructive TEM sample preparation and its limited field of view can also restrict the number of defects that can be observed and hence may impact the statistical limits on estimating defect densities, particularly for materials with lower numbers of dislocations.

There are characterization methods which do not share TEM's requirements for sample preparation. These include atomic force microscopy (AFM), which can offer information on TDs associated with surface pits [3] (often after an etching or decoration treatment) or when terminating in step edges. However, AFM can be sensitive to surface debris and may require extended period of time to image even relatively small areas [4]. Alternatively, for larger area measurements, X-ray diffraction [5] and cathodoluminescence (CL) [6] can provide information on the global material defects densities but can have limitations in terms of resolving individual dislocations.

An alternative to the above methods is the use of electron contrast channelling imaging (ECCI) technique which can be employed within generally available field emission scanning electron microscopes (FE-SEMs) [7-9]. This approach can image defects with resolution of a few nanometers with a micrometer scale field of view, and is neither destructive nor based on direct sample contact. However, in order to obtain the maximum amount of information from these images, a thorough understanding of the contrast mechanisms is required.

For semiconductor materials, ECCI has been used in the forescatter geometry to reveal extended defects and morphological features of GaN samples while also delivering information about crystallographic orientation [10,11]. The electron channelling contrast images obtained in the SEM can provide structural information on dislocations interacting with the sample surface, particularly when obtained in highly diffracting channelling conditions. This information is shown in the form of variation in the electron backscattered (BSE) intensity around a dislocation – or dark-bright signal contrast on the micrograph. Because it can resolve individual dislocations while imaging larger areas (e.g. Nouf-Allehiani et al. [12] for material with TDs having a mean separation of ~200 nm), ECCI is an ideal candidate for both precise and accurate number estimates for a wide range of TD densities (10^6 cm^{-2} – 10^{10} cm^{-2}).

2. The relationship between dislocation strain and ECCI contrast

The image of a single crystal surface in high magnification mode should consist of a constant backscattered electron yield as the near parallel beam is scanned over a small area. Around a dislocation line the crystal structure is distorted, which in turn affects the diffraction of the electron beam. The shift in diffraction behaviour close to the dislocation is observed as a change in the number of backscattered electrons originating from the distorted crystal region and provides direct information about departures from the perfect crystal structure in the ECCI micrograph.

Similarly to the contrast mechanism in TEM described by Hirsch *et al.* [13], the lattice curvature directly affects the distance by which the diffracting reciprocal lattice points deviate from the Bragg condition and is quantified by the deviation parameter s_g. The correction needed to account for the distortion introduced by a lattice defect is then the change in the direction of the incident electron beam ($\mathbf{r_{inc}}$) of the component of the displacement field **u** which is parallel to the reciprocal vector **g** characterizing the diffraction. Tunstall *et al.* [14] showed geometrically that there is a second, smaller correction term which accounts for the change in lattice parameters close to the dislocation.

The corrected deviation parameter expression is shown in equation (1) below:

$$s_g' = s_g + \hat{\boldsymbol{r}}_{\boldsymbol{inc}}.\nabla(\boldsymbol{u}.\boldsymbol{g}) + \theta_B\hat{\boldsymbol{r}}_{\boldsymbol{g}}.\nabla(\boldsymbol{u}.\boldsymbol{g}) = s_g + \beta \tag{1}$$

where θ_B is taken to be the Bragg angle, $r_g = \frac{\boldsymbol{r_g}}{|\boldsymbol{r_g}|}$ is the coordinate in the dislocation frame parallel to **g.**

The new variable β is the sum of all corrections to the deviation parameter due to the defect. If defined in an orthogonal coordinate system it can also be written as:

$$\beta = \frac{\partial u_g}{\partial r_{inc}} + \theta_B \frac{\partial u_g}{\partial g r_g} \tag{2}$$

where u_g is the displacement field in the direction of **g**.

If the displacement field is defined in a Cartesian reference frame in which g is parallel to one of the axes then the corrections terms above can be considered as strain-like components since they measure displacements field gradients. Due to the θ_B weighting factor, the second strain-like term introduced by Tunstall is negligible and can be ignored whenever the first term is non-zero as we will see later. It is these strain-like components that disturb the electron diffraction as compared to a perfect crystal and generate the dark-bright contrast features associated with dislocations in ECCI images.

2.1. Surface effects and why is it challenging to apply the invisibility criterion

We now discuss why, unlike the case for cross-section TEM, the invisibility criteria are not appropriate for dislocation identification in the forescatter geometry of ECCI especially in the absence of high resolution electron channelling patterns (ECPs).

The displacement in an infinite lattice due to a dislocation line of type **a** or **c** can be derived from elasticity theory in the linear regime (see for example Ref. [15]). If the dislocation line interacts in any way with the free surface of the layer, the non-zero stresses at the interface have to be relaxed in order to obtain the full strain picture of the dislocation line. This relaxation in turn introduces extra displacements such that the total displacement at any point in the lattice is a sum of the “infinite-lattice” displacement and that due to the surface relaxation. Yoffe [16] has calculated these surface relaxations due to general dislocations intersecting the surface at an arbitrary angle.

The importance of surface relaxation in the simulation of the electron channelling contrast micrograph has already been discussed by Wilkinson et al. [17] for dislocations running parallel to a nearby surface. Even for the diffraction conditions where the infinite-lattice model gives no ECCI strain-like components, the non vanishing surface strain terms ensure that the net contrast will never be truly zero. This effect will only increase for dislocation lines which penetrate the surface where the non-vanishing surface terms become even more significant. Even in the case where the Burgers vector is perpendicular to the **g** direction, the ECCI sampled strain will be smaller but still not zero.

This reduction in dislocation contrast at the invisibility criteria had been already used in literature [18,19] to show that, at least phenomenologically, the same principle can be applied to ECCI. In practice care is advised when using this approach for the characterisation of dislocations. Unlike TEM which allows reasonable dislocation contrast to be acquired for a significant range of deviations from the Bragg condition, the contrast in ECCI images is optimised at $s_g = 0$ and can change drastically on small variation from that condition. This can determine whether a dislocation is visible or not, even for diffraction conditions where we would expect to see good contrast (see also the discussion in ref. [20]).

*2.2. The effect of tilting the sample when imaging **a** components of TDs*

From equation (2) we can see that the strain profile imaged by ECCI (β) of the **a** characters of a TD normal to the surface is sensitive to variations in the angle of incidence of the electron beam ($\mathbf{r}_{inc}$). This effect is especially strong for edge TDs because they introduce elastic displacement mostly in the plane normal to the dislocation line and present almost no variation along a normally incident beam. Shown schematically in Figure 1, the strain-like component $\partial u_g/\partial r_{inc}$ only contains surface terms and anisotropy effects. Titling the sample (or the beam) translates to rotating the coordinate system in which the ECCI strain is defined, which means the tensor element in the new system will have to contain components from the plane normal to the dislocation line.

The diagram in Figure 1 illustrates this in two dimensions in the case when **b** is parallel to **g**. For a clockwise rotation of θ of the sample around a direction normal to both the dislocation line and its **b**, the first term of β in the new coordinate system will be:

$$\frac{\partial u_g'}{\partial r_{inc}'} = cos^2\theta\,\frac{\partial u_g}{\partial g} + \sin\theta cos\theta\,\frac{\partial u_g}{\partial r_{inc}} \tag{3}$$

where the terms measuring the variation of the displacement field in the beam direction are ignored as they are very small. The first part in the equation above is the variation of the displacement field along **b** (or **g** in this case) and for reasons discussed above will be the dominant term in this strain expression. More about transformation of coordinates will be addressed in next subsection.

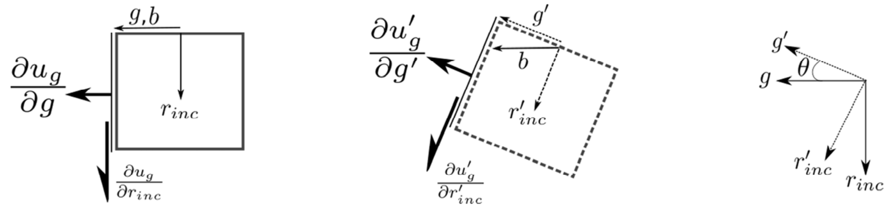

Fig. 1. Diagram of rotation transformation of ECCI strain tensor in two dimensions. A clockwise rotation of θ of the sample is equivalent to the same rotation of the coordinate system in which the strain components are defined.

It is to be expected, then, that tilting the sample will improve the observed contrast of edge dislocations significantly. Figures 2 a)-c) show how a small tilt can significantly change not only the intensity of the sampled strain but also the orientation of its high-low profile. This second effect has to do with the fact that our definition of β contains two strain-like components. Since the variation of displacement field along the line direction – the first term of β – for the **a** character of a threading dislocation is negligibly small, what we observe in Figure 2 a) is purely the second strain-like component introduced by Tunstall. This strain profile closely resembles TEM bright field intensity maps for an edge dislocation normal to the foil surfaced computed by Tunstall et al. [14] with the high-low 'butterfly' lobes oriented on each side of the of the Burgers vector.

However, Tunstall's component is orders of magnitudes less significant than the first β term $\partial u_g/\partial r_{inc}$, which means when the foil is tilted, Tunstall's strain profile will be replaced by the first term's profile. It is remarkable that, in the case when the diffraction vector is aligned parallel with the Burgers vector, any amount of sample tilt will change the direction of the minimum-maximum strain direction from being perpendicular to **b** to being parallel. When the full three dimensional displacement field is considered it becomes apparent that the variation of the field along the extra plane of atoms introduced by the edge dislocation dominates all other factors and this function has its maxima and minima along the Burgers vector. This contrast alignment was observed experimentally and reproduced by simulations for threading dislocations inclined to the surface by Picard et al. [21].

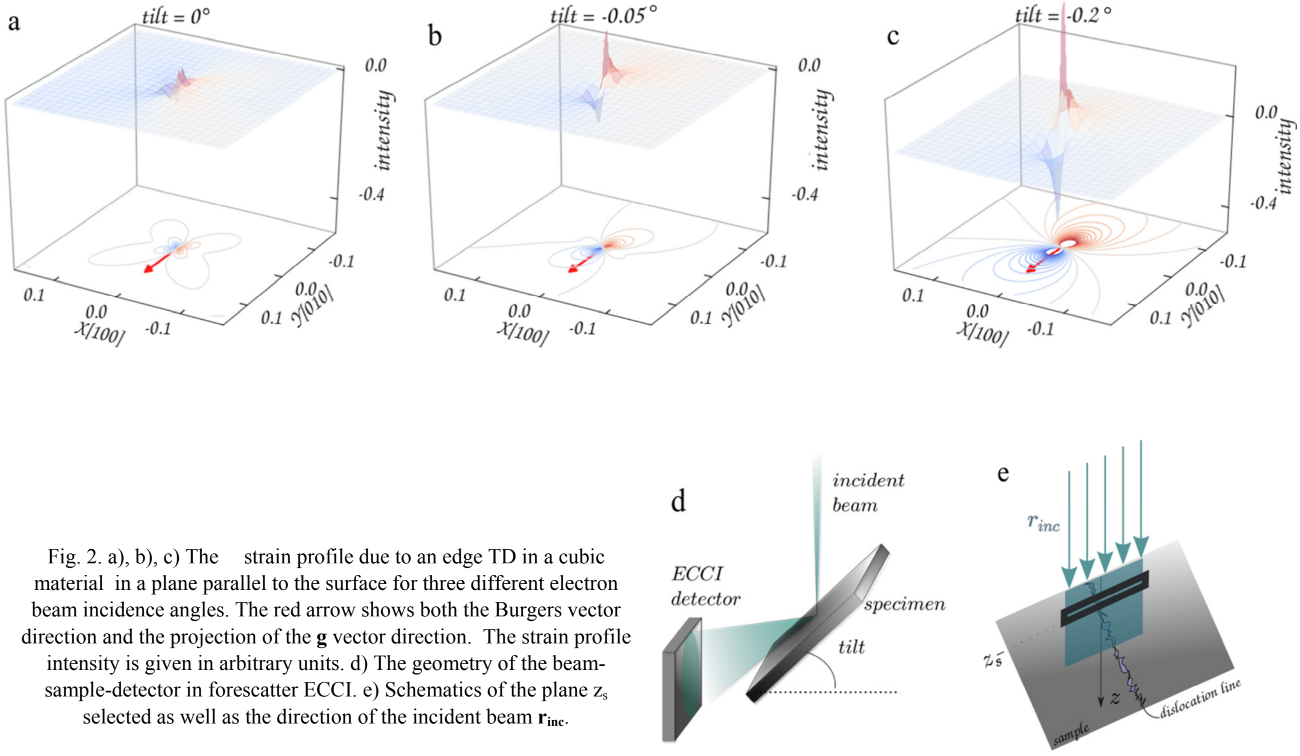

Fig. 2. a), b), c) The strain profile due to an edge TD in a cubic material in a plane parallel to the surface for three different electron beam incidence angles. The red arrow shows both the Burgers vector direction and the projection of the **g** vector direction. The strain profile intensity is given in arbitrary units. d) The geometry of the beam-sample-detector in forescatter ECCI. e) Schematics of the plane z_s selected as well as the direction of the incident beam $\mathbf{r}_{inc}$.

The images in Figure 2 also highlight the ability of forescatter geometry ECCI to access the TD strain profile for cases where plan view imaging might produce low signal to noise features. In general, the higher the tilt, the better the expected contrast of edge TDs will be.

2.3. Coordinate transformations

Equation 1) contains mathematical objects specified in various reference frames and are therefore described using different basis sets. The **g** vectors are described in the reciprocal crystal frame, the displacement field is defined in the dislocation frame and the incident beam and sample orientation are usually given in lab coordinates. The first component of β in equation 1) for instance, can be written to show explicitly the relationship between reference frames, following the notation used by De Graef [22] as:

$$\frac{du(r).g}{dr_{inc}} = (r_{inc})_i^d \frac{\partial u_j^d}{\partial x_i} \mathcal{T}_{jl}^{ds} B_{lm} g_m \tag{4}$$

where Einstein summation convention is used for repeating subscript indices. The superscripts indicate the reference frame in which the expression of the vector is known. B is the reciprocal structure matrix for the unit cell of the material. $\mathcal{T}^{ds}$ is the coordinate transformation matrix which can be applied to a vector described in the dislocation frame (d) in order to be translated in the sample frame (s).

Figure 3 shows the relationship between the lab frame, the sample frame and the dislocation frame as well as the rotations required to orient one with respect to the others. For instance, the sample is rotated clockwise with the angle α_{tilt} about the x axis direction with respect to the lab frame.

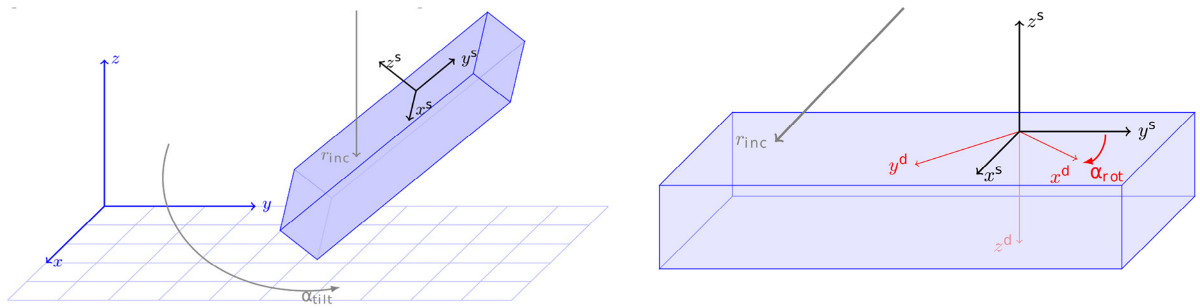

Fig. 3. a) Position of the tilted sample Cartesian frame (denoted by s) and incident beam direction in the lab Cartesian frame used here as the reference frame. b) Relationship between the dislocation reference frame (denoted by d) and the sample reference frame. The crystal frame is defined as an anticlockwise rotation along z^s by α_{rot} and for clarity is not shown here.

If we define the coordinate frames used as meeting the following requirements:

- the sample tilt axis is aligned with its x axis as well as the lab x axis;
- the crystal is non polar so that the crystallographic Cartesian z can be aligned with the sample's z;
- the anticlockwise rotation from the sample frame to the Cartesian crystal frame along z is given by α_{rot};
- the dislocation line frame is defined as the right handed counterpart of the dislocation frame defined by Tunstall [14], such that its z axis is anti-parallel with the crystal frame and the sample frame z axis.

The transformation matrix from the dislocation reference frame to the sample reference frame can be written as:

$$\mathcal{T}_{ds} = \mathcal{R}^z_{(\alpha_{rot})} \mathcal{R}^x_{(\pi)} \mathcal{R}^z_{(3\pi/4)} \tag{5}$$

where $\mathcal{R}^w_{(\theta)}$ is the anticlockwise rotation in a right handed coordinate system looking along w by an angle θ.

These transformations are implemented in this work using the *ReferenceFrame* class from Python's sympy.physics.vector module [23] which proved useful in keeping track of the frames in which vectors and fields are defined as well as the set of rotations between them. The total ECCI strain-like object β is saved as a numerical function of x, y, z position in a Python generated Fortran routine. See supplementary materials at DOI: 10.15129/55fac4ba-b4da-44e1-9fe4-aacfe718c3f1 for a copy of the Python scripts used to perform these simulations.

2.4. Strain profile of ***a*** *components of TDs in wurtzite GaN*

Dislocation analysis of GaN cross sections in TEM shows that the TDs predominantly show pure edge character with the dislocation line lying along the crystallographic c axis and the Burgers vector pertaining to the family $1/3\langle 11\bar{2}0\rangle$ in the four index notation [24].

The ECC images of these types of TD in the forescatter geometry with the film tilted at a high angle will sample strain components that are not parallel to the dislocation line. While the plan view TEM images show TD black-white contrast being aligned perpendicularly to the dislocation Burgers' vector, the geometry of the ECCI highlights a different set of strain components that can align the contrast direction along the Burger vector.

In Figure 4 we show possible strain profiles sampled in a sub-surface plane parallel to the top of the film (similar to Figure 1 for three geometries of orientation of **b** with respect to **g**. In figures 3 a) and c) the maximum variation in strain is aligned with the direction of the Burgers vector. The image in figure 3 b) shows a quasi-invisibility (drastic reduction in strain variation) criterion when the infinite-lattice dislocation strain component dominates, in particular for the case where **g** is perpendicular to **b**.

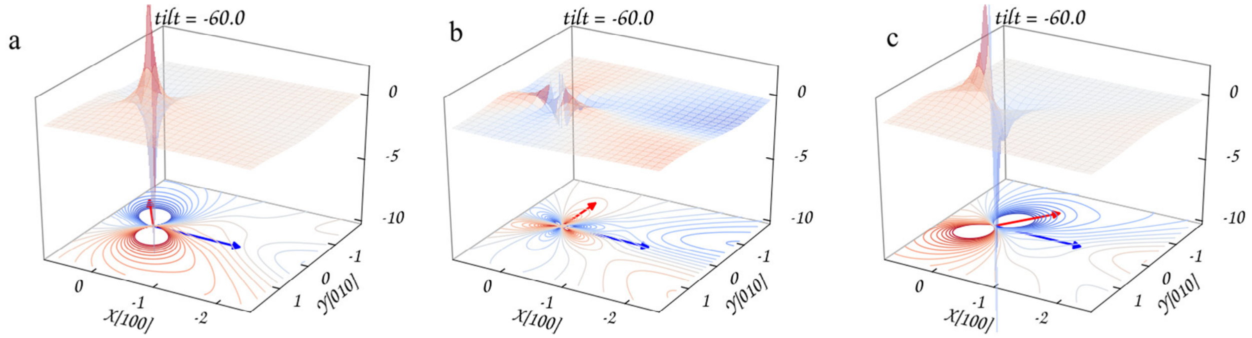

Fig. 4. Accessible strain profiles for an edge TD in wurtzite GaN sampled in a plane parallel to the surface and 1nm below the interface. The sample is tilted 60° from the original horizontal position. The marked red and blue arrows show the direction of the Burgers vector projection and the direction of the projection of the **g** vector respectively. Vector **g** remains the same across the three images while vector **b** is rotated in increments in the same plane such that the angle between the vectors is a) 30° b) 90° c) 150°.

3. Numerical simulation of electron diffraction model

Numerical models of electron diffraction in the SEM tend to follow closely the methodology developed for TEM in the form of Howie-Whelan-Darwin (HWD) equations [25, 26]. These types of equations have already been successfully implemented to predict ECCI dislocation contrast for different dislocation orientations in a number of different material systems [17, 21].

The following physical approximations (described in detail elsewhere [22]) are usually made:

1. High energy electron approximation: the electron energies are large enough so that the second order derivative of the electron wavefunction in the crystal is negligible.
2. The sample is a perfect crystal except at the locations of the dislocations: the electron wavefunction depends only on the penetration depth and is translationally invariant.
3. Column approximation: The HWD equations are solved column-wise and the column are chosen to be big enough to ignore electron scattering between columns.
4. The inelastic scattering processes are included phenomenologically through the introduction of a complex lattice potential.

In this work we follow a similar approach. The dislocation line is placed in the centre of a square mesh. The pixels on the mesh are populated by columns aligned parallel to the incident beam and of length equal to the electron penetration depth. The HWD differential equations are then solved numerically stepwise for each column taking into account the variation of the displacement field along the column calculated previously. We use the Runge-Kutta algorithm available in the *zvode* library [27] for the numerical integrations which, even for stiff equations, can calculate the entire mesh in seconds when using a modern computer.

For the backscattering process we follow the assumption made by Picard *et al.* [21] that the imaged signal comes from those electrons that leave the sample as soon as they suffer their first large angle scattering event. The rest of the scattered electrons (making up the vast majority) will inelastically scatter multiple times on their way back out of the sample losing the diffraction information and only contributing to a uniform background. The backscattering process is stochastic with the probability for an event to occur at any point in the unit cell scaling, to a first approximation, with the square of the atomic number of the elements and their Debye-Waller factor in the crystal.

After the backscattering event the electrons heading towards the detector are projected by yet another coordinate transformation on its surface.

3.1 Edge TD contrast prediction comparison with experiment

Two beam plan view ECC images were acquired using a 50° sample tilt together with electron channelling patterns from the same area for two different crystal rotation: $\mathbf{g}_a$=[-5-7-3] and $\mathbf{g}_b$=[75-3]. This was achieved by tilting the crystal in plane with about 3°. The electron beam energy was 30 keV. The same small area from the two images is shown on the left in Figure 5 a) and b) with the predicted dislocation contrast for three different possible Burgers vectors shown on the right. From the qualitative comparison we can determine which dislocations show similar behaviour to the model cases and assign Burgers vectors.

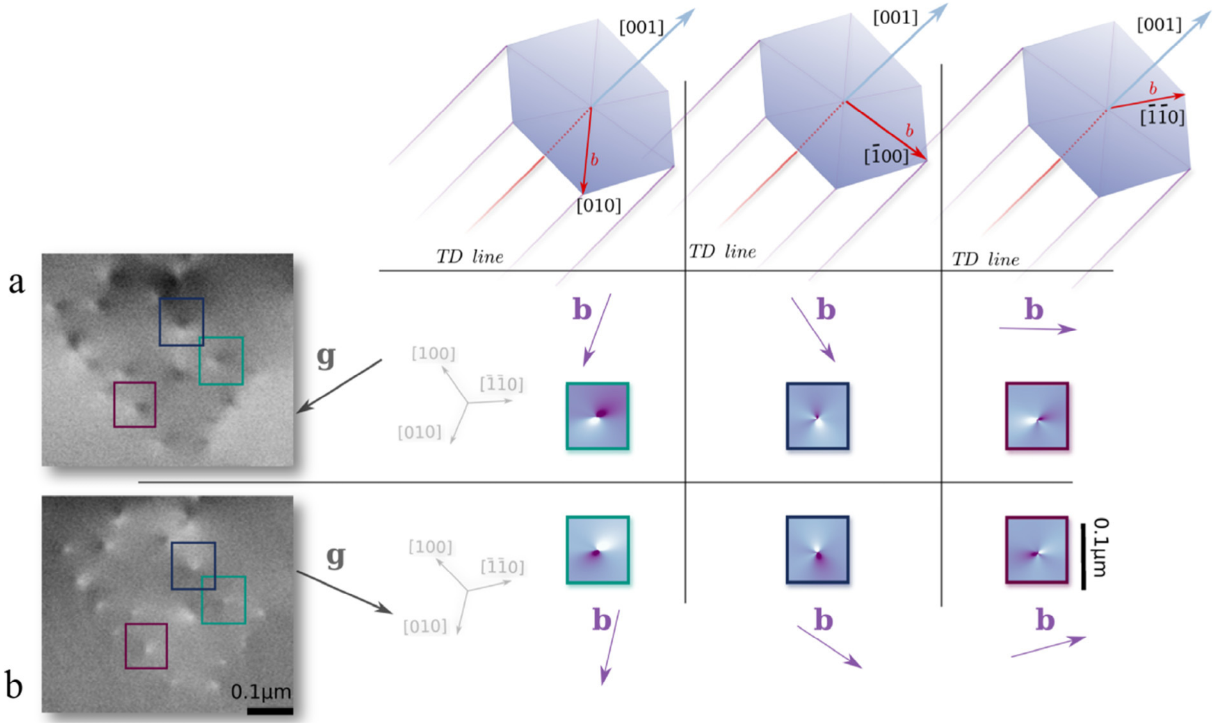

Fig. 5. Experimental versus predicted edge TD dark-bright contrast in ECC images. The two experimental images are from the same area but the crystal has been tilted a few degrees to access the new diffraction condition. The boxes correspond to the contrast produced by an edge TD with **b** = [010] (green box), **b** = [-100] (dark blue box), **b** = [-1-10] (purple box). See details in text. The Bravais three indexes notation was used throughout.

The modelling parameters used are shown in the Table 1. The extinction distances are calculated numerically from the Fourier coefficient of the electrostatic potential of the crystal. The scattering factors of this potential are calculated using Weickenmeier-Kohl parametrization as implemented in EMsoft [32].

For the beam penetration depth calculation needed for the estimation of the diffraction columns integration depth we made use of a continuously slowing down inelastic scattering Monte Carlo model [33].

Table 1. Modelling parameters for edge TD in wurtzite GaN

Parameter	**Symbol**	**Value**	**Reference**
Lattice parameters	a	0.319 nm	[28]
	c	0.519 nm	[29]
Poisson value	ν^w	0.183	[30]
Debye-Waller factors	DWF^{Ga}	0.0027 nm^2	Calculated from [31]
	DWF^{N}	0.0032 nm^2	Calculated from [31]
Extinction distance		29.6 nm	Calculated using [32]
Beam penetration depth	t^{end}	80 nm	Calculated using [33]

The predicted contrasts shown are plotted as variation from the perfect crystal BSE yield. Namely, the calculated BSE intensity is normalised with respect to the BSE yield far away from the dislocation. Normalisation is not used when comparing with the experimental contrast images. The intensity is plotted using the BuPu multi-hue colour scheme of *colorbrewer* [34] with white showing the highest intensity, blue - intermediate values, and dark purple the lowest intensity.

A very similar behaviour to the strain field profile in a plane is observed: the darker-lighter intensity appears to follow the Burgers vector direction. This points towards the fact that a qualitative prediction of TD behaviour can be achieved from a bare strain model correctly 'sampled'. In order to reduce the characterisation uncertainty a larger number of different diffraction conditions should be acquired.

4. Conclusions

ECCI can be used as an alternative to or jointly with the established defect characterisations techniques. Since the usual defect identification procedure is not always appropriate for looking at TDs in ECCI, modelling the contrast predictions becomes critical. The forescatter ECC images provide TD contrast features as cumulative sampled strain components defined in the Cartesian frames selected by the imaging diffraction condition. As these features are unique for different dislocation characters, this technique can be used to identify the type of imaged dislocations by comparison between measured and simulated TDs. We show qualitative agreement for three different Burgers vector edge dislocations contrast against experimental images in two different diffraction conditions.

The scripts and data used for the simulations in this work can be found at DOI: 10.15129/55fac4ba-b4da-44e1-9fe4-aacfe718c3f1.

Acknowledgements

EP would like to acknowledge EPSRC and NPL for funding this work.

CTC, BH and NGK would like to acknowledge the ITN RAINBOW project, Grant Agreement No: PITN-GA-2008-213238 and EPSRC Grant No: EP/D058686/1.

EP would also like to thank Prof. M. De Graef for helpful email conversations.

References

[1] J. S. Speck, S. J. Rosner, Physica B Condens. Matter 273-274 (1999), 24.
[2] T. Hino, S. Tomiya, T. Miyajima, K. Yanashima, S. Hashimoto, M. Ikeda, Appl. Phys. Lett. 76 (2000), 3421.
[3] M. D. Craven, S. H. Lim, F. Wu, J. S. Speck, S. P. DenBaars, Appl. Phys. Lett. 81(2002), 469.
[4] V. N. Koinkar, B. Bhushan, J. Mater. Res. 12 (1997), 3219.

[5] H. Heinke, V. Kirchner, S. Einfeldt, D. Hommel, Appl. Phys. Lett 77 (2000), 2145.
[6] S. J. Rosner, E. C. Carr, M. J. Ludowise, G. Girolami, H. I. Erikson, Appl. Phys. Lett. 70 (1996), 420.
[7] G. Naresh-Kumar, J. Bruckbauer, P. R. Edwards, S. Kraeusel, B. Hourahine, R. W. Martin, M. J. Kappers, M. A. Moram, S. Lovelock, R. A. Oliver, C. J. Humphreys and C. Trager-Cowan, Micros. Microanal. 20 (2014) 55.
[8] G. Naresh-Kumar, D. Thomson., M. Nouf-Allehiani, J. Bruckbauer, P. R. Edwards, B. Hourahine, R. W. Martin, C. Trager-Cowan, Mater. Sci. Semicond. Process. 47(2016), 44.
[9] M. Mansour, J. Guyon, M. A. Crimp, N. Gey, B. Beausir, N. Maloufi, Scr. Mater. (2014)
[10] Y. N. Picard, M. E. Twigg, J.D. Caldwell, C. R. Eddy Jr., P. G. Neudeck, A. J. Trunek, J. A. Powell, Appl. Phys. Lett. 90 (2007), 234101.
[11] C. Trager-Cowan, F. Sweeney, P. W. Trimby, A. P. Day, A. Gholinia, N. -H. Schmidt, P. J, Parbrook, A. J. Wilkinson, I. M. Watson, Phys. Rev. B 75 (2007), 085301.
[12] M. Nouf-Allehiani, G. Kusch, G. Naresh-Kumar, P. R. Edwards, E. Pascal, R. Johnston, S. Kraeusel, B. Hourahine, C. Trager-Cowan, R. W. Martin, F. Mehnke, T. Wernicke, C. Kuhn, J. Enslin, A. Knauer, V. Kueller, M. Weyers, M. Kneissel submitted to Phys. Rev. B
[13] P. B. Hirch, A. Howie, M. J. Whelan, Phil. Trans. A 252 (1960), 667.
[14] W. J. Tunstall, P. B. Hirsch, J.Steeds, Phil. Mag. 9 (1964), 97.
[15] W. T. Read, Dislocations in crystals, McGraw-Hill, New York, 1953.
[16] E. H. Yoffe, Phil. Mag. 6 (1961), 1147.
[17] A. J. Wilkinson, P. B. Hirsch, Phil. Mag. A 72 (1995), 81.
[18] P. Morin, M. Pitaval, D. Besnard, G. Fontaine, Phil. Mag. A 40 (1979), 511.
[19] M. A. Crimp, B. A. Simkin, Phil. Mag. Lett. 81 (2001), 833.
[20] M. A. Crimp, Microsc. Res. Tech 69 (2006), 374.
[21] Y. N. Picard, M. Liu, J. Lammatao, R. Kamaladasa, M. De Graef, Ultramicroscopy 146 (2014), 71.
[22] M. De Graef, Introduction to conventional transmission electron microscopy, Cambridge University Press, New York, 2003.
[23] A. Meurer *et al*., PeerJ Comp. Sci. 3 (2017), 103.
[24] W. Qian, M. Skowronski, M. De Graef, K. Doverspike, L. B. Rowland, D. K. Gaskill, Appl. Phys. Lett. 67 (1995), 1252.
[25] C. G. Darwin, Phil. Mag. 43 (1922), 800.
[26] A. Howie, M. J. Whelan, Proc. Roy. Soc. London A 267 (1962).
[27] A.C. Hindmarsh, A. Odepack, IMACS Trans. Scien. Comp. 1 (1983), 55.
[28] W. Qian, M. Skowronski, G.R. Rohrer, Mater. Res. Soc. Symp. Proc. 423 (1996), 475.
[29] V. Bougrov, M.E. Levinshtein, S.L. Rumyantsev, A. Zubrilov, Properties of Advanced Semiconductor Materials GaN, AlN, InN, BN, SiC, SiGe, John Wiley & Sons, Inc., New York, 2001, 1.
[30] M. A. Moram, Z. H. Barber, C. J. Humphreys, J. Appl. Phys 102 (2007).
[31] M. Schowalter, A. Rosenauer, J. T. Titantah, D. Lamoen, Acta Crystallogr. C 3 (2009), 227.
[32] EMsoft version 3.0, https://github.com/marcdegraef/EMsoft
[33] D. Drouin, A. R. Couture, D. Joly, X. Tastet, V. Aimez, R. Gauvin, Scanning 29 (2007), 92.
[34] colorbrewer 2.0, https://colorbrewer2.org.